

# Thermoelectric transport across a tunnel contact between two charge Kondo circuits: Beyond perturbation theory

T. K. T. Nguyen <sup>1,\*</sup>, H. Q. Nguyen <sup>1</sup> and M. N. Kiselev <sup>2</sup>

<sup>1</sup>*Institute of Physics, Vietnam Academy of Science and Technology, 10 Dao Tan, 118000 Hanoi, Vietnam*

<sup>2</sup>*The Abdus Salam International Centre for Theoretical Physics, Strada Costiera 11, I-34151, Trieste, Italy*

 (Received 21 June 2023; revised 24 January 2024; accepted 5 March 2024; published 18 March 2024)

Following a theoretical proposal on multi-impurity charge Kondo circuits [T. K. T. Nguyen and M. N. Kiselev, *Phys. Rev. B* **97**, 085403 (2018)] and the experimental breakthrough in fabrication of the two-site Kondo simulator [W. Pouse *et al.*, *Nat. Phys.* **19**, 492 (2023)] we investigate a thermoelectric transport through a double-dot charge Kondo quantum nanodevice in the strong coupling operational regime. We focus on the fingerprints of the non-Fermi liquid and its manifestation in the charge and heat quantum transport. We construct a full-fledged quantitative theory describing crossovers between different regimes of the multichannel charge Kondo quantum circuits and discuss possible experimental realizations of the theory.

DOI: [10.1103/PhysRevB.109.115139](https://doi.org/10.1103/PhysRevB.109.115139)

## I. INTRODUCTION

Thermoelectric materials have been investigated in recent years thanks to their ability to generate electricity from waste heat or being used as solid-state Peltier coolers [1]. The mechanism of converting of heat into voltage known as the Seebeck effect [2] is associated with the emergence of the electrostatic potential across the hot and cold ends of the thermocouple [3,4] while no electric current flows through the system. The Peltier effect is manifested by the creation of the temperature difference between the junctions when the electric current flows through the thermocouple.

After theoretical predictions have been suggested that the thermoelectric efficiency could be greatly enhanced through nanostructural engineering in the mid-1990s [5,6], many complex nanostructured materials were studied in both theory and experiment [7–11]. Nano-electric circuits based on one or a few quantum dots (QDs), which are highly controllable and fine tunable, can provide important information about the effects of strong electron-electron interactions, interference effects, and resonance scattering on the quantum charge, spin, and heat transport.

One of the fundamental motivations of the thermoelectric studies is to enhance thermoelectric power (absolute value of the Seebeck coefficient, TP). It is a challenge for both experimental fabrication of devices and theoretical suggestions for efficient mechanisms of heat transfer. In fact, many theoretical investigations showed that the TP of a single electron transistor (SET) was greatly enhanced in comparison with those of bulk materials [12–18] and this has also been realized in experiments [19,20]. Furthermore, the charge Kondo effect [21–26] dealing with the degeneracy of the charge states of the QD (which is similar to the conventional Kondo effect [27–31] but does not require the system to have magnetic degree of

freedom) can be a tool for intensification of the TP of a SET [24,32]. The building block of a charge Kondo circuit (CKC) is a large metallic QD strongly coupled to one (or several) lead(s) through an (or several) almost transparent single-mode quantum point contact(s) [QPC(s)]. In the orthodox charge Kondo theory [21–23], the electron location (namely, in or out of QD) is treated as an isospin variable, while two spin projections of electrons are associated with two (degenerate, in the absence of external magnetic field) conduction channels in the conventional Kondo problem. External magnetic field lifts out the channel degeneracy resulting in a crossover from two-channel Kondo (2CK) regime at the vanishing magnetic field to the single-channel Kondo (1CK) regime at the strong external field [26,33]. As a result, the behavior of the system continuously changes from non-Fermi-liquid (NFL) to the Fermi-liquid (FL) states, respectively. The interplay between NFL-2CK and FL-1CK regimes in thermoelectric transport through the SET has also been investigated in different situations such as: materials with strong spin-orbit interaction [34]; quantum simulators with strong many-body interactions between mobile carriers [36,37]. The proposal of the quantum simulators consisting of two weakly coupled SETs has been suggested in Refs. [35,38]. Recently, the challenging problem of a generalized Wiedemann-Franz (WF) law in the quantum simulators and its connection to the Anderson orthogonality catastrophe has been addressed in Ref. [39]. Beside, the effects of the electron-electron interactions in the charge Kondo simulators have also been considered [40–42]. In those works, the bosonization (and refermionization) method is applied. The charge transport in 1CK and 2CK regimes were studied extensively numerically in Refs. [43–46]. Developing numerical methods for a quantum impurity problem out of equilibrium is still a big challenge. There is a recent progress on the charge Kondo effects by using quantum Monte Carlo (QMC) technique [47–49]. Although the numerical renormalization group [43–46] is more developed and advanced in comparison to the QMC now days, some recent works on

\*nkthanh@iop.vast.vn

QMC on the Keldysh contour [50,51] pave a way for developing new approaches and provide complementary tools for better understanding of both new theoretical models and new experiments with quantum simulators.

Recently, CKCs operated in the integer quantum Hall (IQH) regime have been implemented in breakthrough experiments [52,53]. With the advantage that the number of Kondo channels is determined by the number of QPCs attached to the metallic QD, these experiments have opened an access to investigation of the multichannel Kondo (MCK) problem experimentally. The dominant characteristic of a specific MCK setup is a NFL picture [54–56], which is associated with  $Z_M$  symmetry. For instance, the NFL-2CK [57–59] is explained by Majorana fermions [60,61], the NFL-3CK physics is related to  $Z_3$  parafermions [62–67]. Therefore, switching between  $Z_{2k+1}$  and  $Z_{2k}$  low-temperature fixed points by controlling the reflection amplitudes of the QPCs, can provide a route to investigate the crossovers between states with different parafermion fractionalized zero modes [68].

As a CKC is considered as an artificial quantum simulator for the technology of quantum computer, scaling up the CKCs to clusters or lattices is challenging and it is important to understand the nature of the coupling between neighboring QDs. For this motivation, the experiment [69] has implemented a two-island charge Kondo device in which two QDs are coupled together and each one is also strongly coupled to an electrode through a QPC. The authors investigated the quantum phase transition at the triple point where the charge configurations are degenerate. Being more than the two-impurity Kondo (2IK) model, the two-site charge Kondo circuit (2SCKC) is relevant to the Kondo lattice systems. Furthermore, the deeper theoretical investigation of the strong central coupling of this setup [70,71] in the Toulouse limit showed that a  $Z_3$  parafermion emerging at the critical point, was already present in the experimental device of Ref. [69].

In this work, we revisit the model proposed in Ref. [35], which contains a tunnel contact between two CKCs where each one is set up in either FL or NFL state (see Fig. 1) with a twofold goal. First, we examine the behavior of TP in order to find a mechanism to enhance it. Second, we show the existence of Majorana fermions in this 2SCKC. The approach used in Ref. [35] is based on accounting for the perturbative corrections to the transport off-diagonal coefficients and is limited by the perturbation theory domain of validity (high-temperature regime). These calculations, being very useful for understanding the flow towards the non-Fermi liquid intermediate coupling fixed point, neither become valid at the low-temperature regime, nor shed a light on reduction of the symmetry due to the emergence of the Majorana (parafermionic) states. The main idea of this work is to develop a controllable and reliable approach for the quantitative description of the Fermi-to-non-Fermi liquid crossovers and interplay around the intermediate coupling fixed points. It therefore provides a complementary study of the model [35] and completes the theory of thermoelectrics in 2SCKCs. The new energy scale associated with the inverse lifetime of the emergent Majorana fermions controls four different regimes of thermoelectric transport based on the window of parameters.

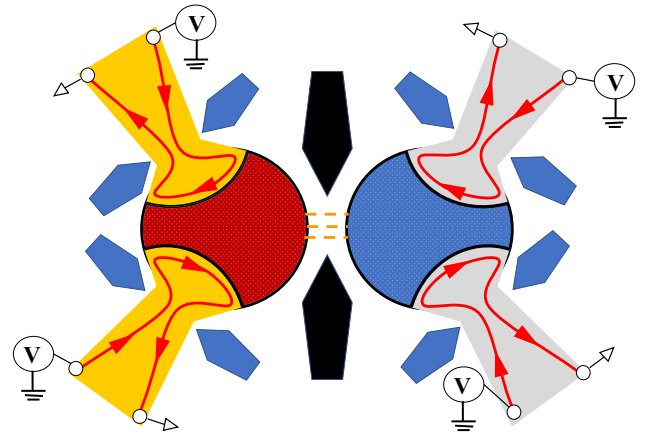


FIG. 1. Schematic of a weak link between two charge Kondo circuits (CKC). Each circuit consists of a large metallic island (QD), which is embedded into two-dimensional electron gas (2DEG) and connects to two large electrodes through the single-mode quantum point contacts (QPCs). The 2DEG (plain area) is in the integer quantum Hall regime  $\nu = 1$ . The red line with arrows denotes the chiral edge mode, which backscatters at the center of the narrow constriction. The QPCs are fine tuned by field effects in split gates (blue boxes) to different regimes. We name the QPCs in the left CKC as QPC<sub>11</sub>, QPC<sub>12</sub> and the QPCs in the right CKC as QPC<sub>21</sub>, QPC<sub>22</sub>. The right CKC (gray color) is at the reference temperature  $T$  while the left circuit (orange color) is at higher temperature  $T + \Delta T$ .

The paper is organized as follows. We briefly describe the proposed experimental setup and general equations for the thermoelectric coefficients in Sec. II. The Sec. III represents the correlation function in different cases. The main results are represented in Sec. IV. We discuss the results and conclude our work in Sec. V.

## II. PROPOSED EXPERIMENTAL SETUP AND GENERAL EQUATIONS FOR THE THERMOELECTRIC COEFFICIENTS

### A. Proposed experimental setup

We consider a 2SCKC device (see Fig. 1) formed by two CKCs describing a very recent experiment [69]. The building block for each CKC is a QD-QPC structure implemented in experiment [52]. The QD is a large metallic island (the dark-red and blue cross-hatched areas surrounded by the black lines) electronically connected to a two-dimensional electron gas (2DEG, the orange and gray continuous areas). The 2DEG is connected to two large electrodes through two QPCs. Applying a strong magnetic field perpendicular to the 2DEG plane can control the 2DEG in the IQH regime at the filling factor  $\nu = 1$ . The QPCs are fine tuned (by field effects in the split gates illustrated by the blue boxes) to the high transparency regime corresponding to weak backscattering of the chiral edge mode (red solid lines with arrows). We investigate the regime of equal reflection amplitudes at two QPCs in each CKC:  $|r_{11}| = |r_{12}| = |r_1|$  and  $|r_{21}| = |r_{22}| = |r_2|$ . Therefore, each CKC is a 2CK setup. Indeed, the CKC can be tuned into a 1CK model by simply deactivating one of the two QPCs in it. These two CKCs are connected together by a weak tunneling (barrier, weak link) between two QDs. In order to study the

thermoelectric transport through the 2SCKC system, the left CKC is set up at higher temperature  $T + \Delta T$  in comparison with the right circuit, which is at temperature  $T$ . The temperature drops at the central weak link.

### B. General formulas for the thermoelectric coefficients

In order to study the thermoelectric effects at the weak link between two QDs in the linear response regime  $[\Delta T, e\Delta V] \ll T$  (we adopt the units  $\hbar = c = k_B = 1$ ), we consider both the charge current  $I_e$  and the heat current  $I_h$  across the tunnel contact [72]:

$$\begin{pmatrix} I_e \\ I_h \end{pmatrix} = \begin{pmatrix} G & G_T \\ TG_T & G_H \end{pmatrix} \begin{pmatrix} \Delta V \\ \Delta T \end{pmatrix}, \quad (1)$$

where  $G, G_T, G_H$  are the electric conductance, thermoelectric coefficient, and thermal coefficient, correspondingly. The computations for the above currents involve the local density of states (DoS)  $\nu_j(\epsilon)$  of QD  $j$  at the weak link through the transport integrals:

$$\mathcal{L}_n(T) = \frac{1}{4T} \int_{-\infty}^{\infty} \frac{\epsilon^n}{\cosh^2(\frac{\epsilon}{2T})} \mathcal{T}(T, \epsilon) d\epsilon, \quad n = 0, 1, 2, \quad (2)$$

where

$$\mathcal{T}(T, \epsilon) = 2\pi e^2 |t|^2 \nu_1(T, \epsilon) \nu_2(T, \epsilon) \quad (3)$$

is the transmission coefficient, and  $|t|$  is the tunneling amplitude of the central link. The thermoelectric coefficients are related to the transport integrals as  $G = \mathcal{L}_0$ ,  $G_T = -\mathcal{L}_1/T$ , and  $G_H = \mathcal{L}_2/T$ . In the spirits of Matveev-Andreev theory [24], the DoS  $\nu_j(T, \epsilon)$  is related to the correlation function  $K_j(1/2T + it)$  as

$$\nu_j(T, \epsilon) = \nu_{0,j} T \cosh\left(\frac{\epsilon}{2T}\right) \int_{-\infty}^{\infty} \frac{e^{i\epsilon t} K_j(\frac{1}{2T} + it)}{\cosh(\pi T t)} dt, \quad (4)$$

where  $\nu_{0,j}$  stands for the DoS of the QD $_j$  which is no longer renormalized by the electron-electron interactions, while the correlation function  $K_j(1/2T + it)$  characterizes for these interactions. The details of the derivative procedure for electric conductance and thermoelectric coefficient have been represented in Refs. [35,38]. At the end, one can write the formulas of the electric conductance, thermoelectric coefficient, and thermal conductance as [72]:

$$G = \frac{\partial I_e}{\partial \Delta V} \Big|_{\Delta T=0} = \frac{\pi}{2} G_C T \int_{-\infty}^{\infty} \frac{dt}{\cosh^2(\pi T t)} \times K_1\left(\frac{1}{2T} + it\right) K_2\left(\frac{1}{2T} - it\right), \quad (5)$$

$$G_T = \frac{\partial I_e}{\partial \Delta T} \Big|_{\Delta V=0} = -\frac{i\pi G_C}{4e} \int_{-\infty}^{\infty} \frac{dt}{\cosh^2(\pi T t)} \times \left\{ \left[ \partial_t K_1\left(\frac{1}{2T} + it\right) \right] K_2\left(\frac{1}{2T} - it\right) - K_1\left(\frac{1}{2T} + it\right) \left[ \partial_t K_2\left(\frac{1}{2T} - it\right) \right] \right\}, \quad (6)$$

and

$$\mathcal{K} = \frac{\partial I_h}{\partial \Delta T} \Big|_{I_e=0} = G_H - T \frac{G_T^2}{G}, \quad (7)$$

with  $G_H$  is thermal coefficient, which is expressed as

$$G_H = \frac{\partial I_h}{\partial \Delta T} \Big|_{\Delta V=0} = \frac{\pi G_C}{2e^2} \int_{-\infty}^{\infty} dt \times \left\{ \frac{\pi^2 T^2 [2 - \cosh^2(\pi T t)]}{\cosh^4(\pi T t)} K_1\left(\frac{1}{2T} + it\right) \times K_2\left(\frac{1}{2T} - it\right) + \frac{1}{\cosh^2(\pi T t)} \partial_t K_1\left(\frac{1}{2T} + it\right) \partial_t K_2\left(\frac{1}{2T} - it\right) \right\}, \quad (8)$$

where  $G_C = 2\pi e^2 \nu_{0,1} \nu_{0,2} |t|^2$  is a conductance of the central (tunnel) area assuming that the electrons in the QDs are non-interacting. The TP in the linear regime is defined at  $I_e = 0$  as

$$S = -\frac{\Delta V}{\Delta T} \Big|_{I_e=0} = \frac{G_T}{G}. \quad (9)$$

The definition of the figure of merit  $ZT$ , which characterizes the quality of a thermoelectric material, reads

$$ZT = \frac{GT S^2}{\mathcal{K}}. \quad (10)$$

One should notice that the equation for the thermal conductance  $\mathcal{K}$  (7) contains both the diagonal and the off-diagonal Onsager coefficients [72]. The thermal conductance is connected to the electric conductance  $G$  (typically, in the low-temperature regime) by a universal constant called the Lorenz number [73,74]:

$$\frac{\mathcal{K}}{GT} = L_0 = \frac{\pi^2}{3e^2}. \quad (11)$$

Connection between electric and thermal conductances (11) is established by the WF law. The validity of WF law is attributed to the fact that both charge and heat are transferred by the same quasiparticles. In some strongly correlated systems, however, the  $\mathcal{K}/(GT)$  is deviated from  $L_0$  still remaining the universal number [39,75]. Thus, the generalized WF law is applied for description of such systems. The computation of thermoelectric coefficients in Eqs. (5), (6), and (8) [76] requires the explicit form of the correlation functions  $K_{1,2}(1/2T \pm it)$ .

### III. CORRELATION FUNCTION $K_j(\tau)$

In the Matveev-Andreev spirits, the time-ordered correlation function  $K_j(\tau) = \langle T_\tau F(\tau) F^\dagger(0) \rangle$  ( $T_\tau$  is the time-ordering operator, the imaginary time  $t$  runs from 0 to  $\beta = 1/T$ ) accounts for interaction effects in QDs. The operator  $F^\dagger(0)$  increases number of electrons entering the QD $_j$  through the weak link (characterized by operator  $\hat{n}$ ) from 0 to 1 at time  $t = 0$  and  $F(\tau)$  decreases it back to 0 at time  $t = \tau$ , one can replace  $\hat{n}$  by  $n_{j\tau}(t) = \theta(t)\theta(\tau - t)$  with  $\theta(t)$  is the unit step function. Therefore, the correlation function  $K_j(\tau)$  is computed through the functional integration over the bosonic fields  $K_j(\tau) = Z_j(\tau)/Z_j(0)$  [24].

### A. 1CK case: Perturbative solution

In the case one CKC is settled down in the FL-1CK state by decoupling one of the two QPCs, the functional integral writes

$$Z_j(\tau) = \int \mathcal{D}\phi_j \exp[-\mathcal{S}_{0,j} - \mathcal{S}_{C,j}(\tau) - \mathcal{S}_{s,j}], \quad (12)$$

where  $\mathcal{S}_{0,j}$ ,  $\mathcal{S}_{C,j}$ , and  $\mathcal{S}_{s,j}$  are Euclidean actions describing the free (noninteracting) one-dimensional Fermi gas, Coulomb blockade in the QD and the backscattering at the QPC of the CKC  $j$ , respectively. They are written as [24,77,78]

$$\mathcal{S}_{0,j} = \frac{v_F}{2\pi} \int_0^\beta dt \int dx \left[ \frac{(\partial_t \phi_j)^2}{v_F^2} + (\partial_x \phi_j)^2 \right], \quad (13)$$

$$\mathcal{S}_{C,j} = E_{C,j} \int_0^\beta dt \left[ n_{j\tau}(t) + \frac{1}{\pi} \phi_j(0, t) - N_j \right]^2, \quad (14)$$

$$\mathcal{S}_{s,j} = -\frac{2D}{\pi} |r_j| \int_0^\beta dt \cos[2\phi_j(0, t)]. \quad (15)$$

with  $\phi_j$  representing the bosonic field at the QPC of the CKC  $j$ , and  $v_F$  is the Fermi velocity,  $E_{C,j}$  is the charging energy of the QD  $j$ ,  $N_j$  is the normalized dimensionless gate voltage, controlled by plunger gates (not shown in Fig. 1), and  $D$  is a bandwidth. One should notice that the bosonic field describing the electrons moving through the constriction is blocked by the Coulomb interaction in the QD. Therefore,  $Z_j(\tau)$  can be computed perturbatively over  $|r_j|$  for the small backscattering at the QPC ( $|r_j| \ll 1$ ), and the correlation function  $K_j(\tau)$  then is

$$K_j(\tau) = \left( \frac{\pi^2 T}{\gamma E_{C,j}} \right)^2 \frac{1}{\sin^2(\pi T \tau)} [1 - 2\gamma \xi |r_j| \cos(2\pi N_j) + 4\pi^2 \xi \gamma |r_j| \frac{T}{E_{C,j}} \sin(2\pi N_j) \cot(\pi T \tau)], \quad (16)$$

with  $\gamma = e^C$ ,  $C \approx 0.577$  is Euler's constant,  $\xi = 1.59$  is a numerical constant [24].

### B. Symmetric 2CK case: Nonperturbative solution

For convenient calculation later, one can define the variables  $\phi_{j,\rho/\sigma} = \phi_{j,1} \pm \phi_{j,2}$  so-called charge/spin fields where  $\phi_{j,\alpha}$  ( $\alpha = 1, 2$ ) represents the bosonic field at the QPC  $\alpha$  of the CKC  $j$ . The functional integral in this case is written as:

$$Z_j(\tau) = \prod_{\lambda=\rho,\sigma} \int \mathcal{D}\phi_{j,\lambda} \exp[-\mathcal{S}_{0,j} - \mathcal{S}_{C,j}(\tau) - \mathcal{S}_{s,j}], \quad (17)$$

where  $\mathcal{S}_{0,j}$ ,  $\mathcal{S}_{C,j}$ , and  $\mathcal{S}_{s,j}$  are Euclidean actions describing the free Fermi liquid, Coulomb blockade in the QD and the backscattering at the QPCs of the CKC  $j$ , respectively. The action  $\mathcal{S}_{0,j}$  is presented as a sum of two independent actions

$$\mathcal{S}_{0,j} = \sum_{\lambda=\rho,\sigma} \frac{v_F}{2\pi} \int_0^\beta dt \int dx \left[ \frac{(\partial_t \phi_{j,\lambda})^2}{v_F^2} + (\partial_x \phi_{j,\lambda})^2 \right]. \quad (18)$$

The Coulomb blockade action  $\mathcal{S}_{C,j}$  in bosonic representation reads [77]

$$\mathcal{S}_{C,j} = E_{C,j} \int_0^\beta dt \left[ n_{j\tau}(t) + \frac{\sqrt{2}}{\pi} \phi_{j,\rho}(0, t) - N_j \right]^2. \quad (19)$$

The contribution  $\mathcal{S}_{s,j}$  in the action of each CKC characterizes the weak backscattering at the QPCs is

$$\mathcal{S}_{s,j} = -\frac{2D}{\pi} |r_j| \int_0^\beta dt \cos[\sqrt{2}\phi_{j,\rho}(0, t)] \times \cos[\sqrt{2}\phi_{j,\sigma}(0, t)]. \quad (20)$$

In the absence of backscattering  $|r_j| = 0$ , the functional integral Eq. (17) is Gaussian. The correlator  $K_j^{(0)}(\tau) \equiv K_j(\tau)|_{r=0} = K_{j,\rho}(\tau)$  is computed at low temperature  $T \ll E_C$  and at  $\tau \gg E_C^{-1}$ :

$$K_{j,\rho}(\tau) = \frac{\pi^2 T}{2\gamma E_{C,j}} \frac{1}{|\sin(\pi T \tau)|}. \quad (21)$$

The perturbative results (see Ref. [24]) showed that the thermoelectric properties of the system are controlled by charge and spin fluctuations at low frequencies (below  $E_{C,j}$ ). One should notice that the effect of small but finite  $|r_j|$  on the charge modes is negligible in comparison with the Coulomb blockade but it changes the low-frequency dynamics of the unblocked spin modes dramatically. The correlation function can be split into charge and spin components as  $K_j(\tau) = K_{j,\rho}(\tau)K_{j,\sigma}(\tau)$ , with  $K_{j,\sigma}(\tau) = Z_{j,\sigma}(\tau)/Z_{j,\sigma}(0)$ . We simply replace the  $\cos[\sqrt{2}\phi_{j,\rho}(0, t)]$  in action Eq. (20) by the  $\langle \cos[\sqrt{2}\phi_{j,\rho}(0, t)] \rangle_\tau = \sqrt{2\gamma E_{C,j}/\pi D} \cos[\pi N_j - \chi_{j\tau}(t)]$ , with  $\chi_j(t) = \pi n_{j\tau}(t) + \delta\chi_{j\tau}(t)$ ,  $\delta\chi_{j\tau}(t) \approx (\pi^2 T/2E_{C,j})[\cot(\pi T(t-\tau)) - \cot(\pi T t)]$  and obtain the effective action for the spin degrees of freedom in the form

$$\mathcal{S}_{\tau j} = \int dx \int_0^\beta dt \frac{v_F}{2\pi} \left[ \frac{(\partial_t \phi_{j,\sigma})^2}{v_F^2} + (\partial_x \phi_{j,\sigma})^2 \right] - \int_0^\beta dt \sqrt{\frac{4D}{v_F}} \tilde{\lambda}_{j\tau}(t) \cos[\sqrt{2}\phi_{j,\sigma}(0, t)], \quad (22)$$

where

$$\tilde{\lambda}_{j\tau}(t) = \Lambda_j (-1)^{n_\tau(t)} \cos[\pi N_j - \delta\chi_{j\tau}(t)], \quad \Lambda_j = |r_j| \sqrt{\frac{2\gamma v_F E_{C,j}}{\pi D}}. \quad (23)$$

After performing the refermionization, our model [as shown in Eq. (22)] is mapped onto an effective Anderson model, which is described by Hamiltonian

$$H_{j,\tau}^{\text{eff}}(t) = \int [v_F k c_{j,k}^\dagger c_{j,k} - \tilde{\lambda}_{j\tau}(t) (c + c^\dagger)(c_{j,k} - c_{j,k}^\dagger)] dk, \quad (24)$$

in which the operators  $c_{j,k}^\dagger$  and  $c_{j,k}$  satisfying the anticommutation relations  $\{c_{j,k}, c_{j,k'}^\dagger\} = \delta(k - k')$  create and destroy chiral fermions;  $c$  is a local fermionic annihilation operator anticommuting with  $c_{j,k}^\dagger$  and  $c_{j,k}$ . We see that the model is free and equivalent to a resonant level model where the leads

are coupled to Majorana fermion  $\eta = (c + c^\dagger)/\sqrt{2}$  on the impurity. The time-dependent Hamiltonian (24) can be split into  $H_{j,0}^{\text{eff}} + H'_{j,\tau}(t)$  by replacing  $\tilde{\lambda}_{j\tau}(t) \rightarrow \tilde{\lambda}_{j\tau}(t)/(-1)^{n_\tau(t)}$ . The time-independent Hamiltonian part  $H_{j,0}^{\text{eff}}$  is  $H_{j,\tau=0}^{\text{eff}}$  while the correction is

$$H'_{j,\tau}(t) = 2\Lambda_j \{ \cos[\pi N_j] - \cos[\pi N_j - \delta\chi_{j\tau}(t)] \} \eta \zeta, \quad (25)$$

with  $\zeta = \int_{-\infty}^{\infty} (c_{j,k} - c_{j,k}^\dagger) dk / \sqrt{2}$  describes the Majorana fermion of the leads in the resonant level model. Our solution, being nonperturbative in  $|r_j|$  and accounting for low-frequency dynamics of the spin modes, leads to the appearance of the Kondo-resonance width  $\Gamma_j$  in the vicinity of Coulomb peaks

$$\Gamma_j(N_j) = \frac{8\gamma E_{C,j}}{\pi^2} |r_j|^2 \cos^2(\pi N_j). \quad (26)$$

We then compute the correlation function straightforwardly and obtain the zero order in  $|r_j|$  term corresponding to the Hamiltonian part  $H_{j,0}^{\text{eff}}$  as

$$K_j^{(0)} \left( \frac{1}{2T} + it \right) = \frac{\pi T \Gamma_j}{\gamma E_{C,j}} \frac{1}{\cosh(\pi T t)} \times \int_{-\infty}^{\infty} \frac{e^{\omega(1/2T+it)}}{(\omega^2 + \Gamma_j^2)(1 + e^{\omega/T})} d\omega, \quad (27)$$

and the first-order term when the correction Hamiltonian part  $H'_{j,\tau}(t)$  is taken into account, is

$$K_j^{(1)} \left( \frac{1}{2T} + it \right) = -\frac{4T}{E_{C,j}} \frac{|r_j|^2 \sin(2\pi N_j)}{\cosh(\pi T t)} \times \ln \left( \frac{E_{C,j}}{T + \Gamma_j} \right) \int_{-\infty}^{\infty} d\omega \times \frac{\omega e^{\omega(1/2T+it)}}{(\omega^2 + \Gamma_j^2)(1 + e^{\omega/T})}. \quad (28)$$

One should notice that if the correlation function  $K_j(\tau)$  is considered at the zeroth- $|r_j|$  order  $K_j^{(0)}$  in the Eq. (27), the DoS of a charge Kondo circuit  $j$  is an even function of the energy  $\epsilon/\Gamma_j$ , while the contribution to DoS due to the first order in  $|r_j|$  term  $K_j^{(1)}$  in the Eq. (28) is an odd function of energy. The DoS of a CKC is shown in Fig. 2. In the regime of small compared to the temperature energies (in comparison to the Kondo temperature, which is  $E_{C,j}$  in the charge Kondo model) the DoS are analytic functions obeying a Taylor expansion  $v_j/v_{0,j} \propto a_j(|r_j|, T) + b_j(|r_j|, T)(\epsilon/E_{C,j}) + c_j(|r_j|, T)(\epsilon/E_{C,j})^2 + d_j(|r_j|, T)(\epsilon/E_{C,j})^3 + \dots$  (here  $a_j, b_j, c_j, d_j$  are constant depending on the system parameters) [see the insert of Fig. 2] while  $v_j/v_{0,j} \propto |\epsilon/E_{C,j}|$  in the other regime of energy. The latter is explained based on the orthogonality catastrophe [23,39]. The symmetry and asymmetry of the contributions originated from  $K_j^{(0)}$  and  $K_j^{(1)}$  to the DoS implies that it is enough to take into account  $K_j^{(0)}$  in order to compute  $G$  and  $G_H$  but it is necessary to consider  $K_j^{(1)}$  when one calculates  $G_T$  [see Eqs. (2), (3)]. The formulas (27) and (28) will be used to calculate the thermoelectric coefficients in the next section.

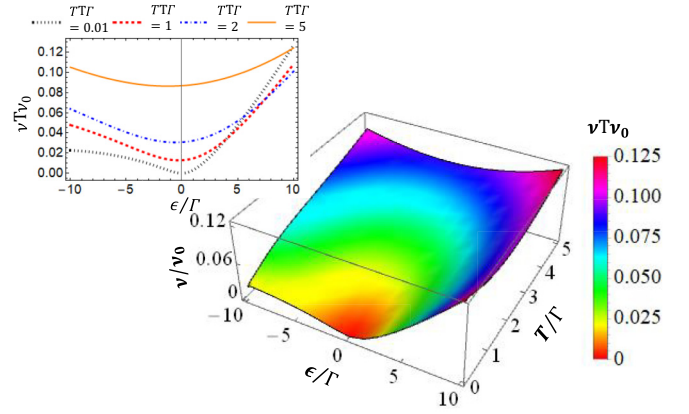


FIG. 2. The density of states (DoS) of a charge Kondo circuit  $v/v_0$  is plotted. Both the even function of time correlation functions  $K_j^{(0)}$  given by the Eq. (27) and the odd function of time  $K_j^{(1)}$  given by Eq. (28) being proportional to the second power of the particle-hole symmetry breaking parameter  $|r|$  are taken into account. The DoS is plotted as a function of ratio of energy to the Kondo resonance width  $\epsilon/\Gamma$  and ratio of temperature to the Kondo resonance width  $T/\Gamma$  (we choose  $N_1 = N_2 = N = 0.42$ ,  $|r_1|^2 = |r_2|^2 = |r|^2 = 0.12$ ,  $E_{C,1} = E_{C,2} = E_C$ , and therefore  $\Gamma_1 = \Gamma_2 = \Gamma$ ). Insert: zoomed in DoS as the function of ratio of energy to the Kondo resonance width  $\epsilon/\Gamma$  at different temperatures  $T/\Gamma = 0.01, 1, 2, 5$  corresponding to the black dotted, red dashed, blue dot-dashed, and orange lines.

## IV. MAIN RESULTS

Going beyond the perturbation theory assuming smallness of the reflection amplitudes of the QPCs as represented in Ref. [35], we develop a controllable and reliable approach for the quantitative description of the Fermi-to-non-Fermi liquid crossovers and interplay around the intermediate coupling fixed points in this work.

### A. Weak coupling between single- and two-channel charge Kondo circuits

To begin with description of the weakly coupled single- and two-channel Kondo simulators we consider the circuit consisting of the left CKC being in the FL-1CK state and the right CKC operating in the NFL-2CK state. We apply the correlation functions  $K_1(\frac{1}{2T} + it)$  and  $K_2(\frac{1}{2T} - it)$  as shown in Eqs. (16) and (27)–(28), respectively. The electric conductance is given by

$$G = \frac{\pi^2 G_C T^3}{96 \gamma^3 E_{C,1}^2 E_{C,2}} F_G \left( \frac{\Gamma_2}{T} \right), \quad (29)$$

with  $F_G$  is a dimensionless function describing the interplay between the width of the Kondo resonance of the right CKC  $\Gamma_2$  and the temperature  $T$ . It is expressed as

$$F_G \left( p_2 = \frac{\Gamma_2}{T} \right) = \int_{-\infty}^{\infty} du J(p_2, u), \quad (30)$$

$$J(p_2, u) = \frac{p_2 [u^2 + \pi^2] [u^2 + 9\pi^2]}{\cosh^2 \left( \frac{u}{2} \right) [u^2 + p_2^2]}. \quad (31)$$

The thermoelectric coefficient  $G_T$  is given by

$$\begin{aligned}
 G_T = & -\frac{\pi^5 \xi G_C}{72e\gamma^2} |r_1| \sin(2\pi N_1) \frac{T^4}{E_{C,1}^3 E_{C,2}} F_G\left(\frac{\Gamma_2}{T}\right) \\
 & -\frac{\pi^3 \xi G_C}{180e\gamma^2} |r_1| \sin(2\pi N_1) \frac{T^4}{E_{C,1}^3 E_{C,2}} F_T\left(\frac{\Gamma_2}{T}\right) \\
 & -\frac{\pi G_C}{40e\gamma^2} |r_2|^2 \sin(2\pi N_2) \\
 & \times \frac{T^4}{E_{C,1}^2 E_{C,2} \Gamma_2} \ln\left(\frac{E_{C,2}}{T + \Gamma_2}\right) F_T\left(\frac{\Gamma_2}{T}\right), \quad (32)
 \end{aligned}$$

with

$$F_T(p_2) = \int_{-\infty}^{\infty} du u^2 J(p_2, u). \quad (33)$$

Following the discussion in Ref. [35], based on the perturbative solution, the Seebeck effect on a weak link between 1CK and 2CK is characterized by the interplay between the Fermi- and non-Fermi-liquid regimes (see Eq. (24) in the Ref. [35]). However, this competition is appreciable only at sufficiently high temperatures  $T \gg \Gamma_2$ . At the very low temperatures,  $T \ll \Gamma_2$ , the Fermi-liquid regime characterized by the linear dependence of the TP as the function the temperature holds.

### 1. $T \gg \Gamma_2$ limit: Fermi liquid on the left and non-Fermi-liquid on the right CKC

At temperature regime  $T \gg \Gamma_2$ , we get  $F_G(p_2 = \Gamma_2/T \rightarrow 0) = 9\pi^5$  and  $F_T(p_2 \rightarrow 0) = 256\pi^4 p_2/5$ . Naturally, the expression in Eq. (32) reproduces the perturbative result (see Eq. (23) of Ref. [35]). The equation for TP is thus similar to the formula (24) in Ref. [35]:

$$\begin{aligned}
 S = & -\frac{4\pi^3 \xi \gamma}{3e} |r_1| \frac{T}{E_{C,1}} \sin(2\pi N_1) \\
 & -\frac{256\gamma}{75\pi^2 e} |r_2|^2 \ln\left(\frac{E_{C,2}}{T}\right) \sin(2\pi N_2). \quad (34)
 \end{aligned}$$

The crossover temperature  $\tilde{T}$  separating two contributions ( $T$ -linear FL and  $\log T$  NFL) in the TP is defined as follows:

$$\ln\left(\frac{E_{C,2}}{\tilde{T}}\right) \frac{E_{C,1}}{\tilde{T}} = \frac{25\pi^5 \xi}{256} \frac{|r_1|}{|r_2|^2}. \quad (35)$$

If  $\Gamma_2 \ll T \ll \tilde{T}$ , NFL-2CK behavior of the TP is predicted to be dominant. In the opposite limit,  $T \gg \tilde{T} \gg \Gamma_2$ , the FL-1CK regime with the weak NFL-2CK corrections is expected.

### 2. $T \ll \Gamma_2$ limit: Fermi-liquid regime

At temperature regime  $T \ll \Gamma_2$ , we get  $F_G(p_2 = \Gamma_2/T \gg 1) = 256\pi^4/5p_2$  and  $F_T(p_2 \gg 1) = 256\pi^6/7p_2$ . The expression in Eq. (32) produces the linear in temperature term. The FL picture is thus described through the property of TP as

$$\begin{aligned}
 S = & -\frac{12\pi^3 \xi \gamma}{7e} \left[ \frac{|r_1|}{E_{C,1}} \sin(2\pi N_1) \right. \\
 & \left. + \frac{\tan(\pi N_2)}{4\gamma \xi E_{C,2}} |r_2|^2 \ln\left(\frac{E_{C,2}}{\Gamma_2}\right) \right] T. \quad (36)
 \end{aligned}$$

In summary, in the regime of the weak coupling between single- and two-channel charge Kondo circuits, there exist two energy scales: the Kondo width  $\Gamma_2 \sim (8\gamma/\pi^2)E_{C,2}|r_2|^2$  and the crossover temperature  $\tilde{T}$ . When the condition  $0 < \Gamma_2 < \tilde{T} < E_{C,2}$  holds, the domain of validity for the Fermi-liquid regime is significantly larger compared to the non-Fermi-liquid domain. The results discussed in this section are completely consistent with the perturbative results represented in Ref. [35]. The mixed FL + NFL operational regime of the thermopower given by Eq. (34) can only be achieved at the intermediate temperatures restricted by the condition  $(8\gamma/\pi^2)E_{C,1}|r_1|^2 \ll T \ll (E_{C,1}, E_{C,2})$ .

### B. Weak coupling between two-site two-channel charge Kondo circuits

To compute electric conductance through weakly linked two-site two-channel charge Kondo circuit it is sufficient to take into account only even in time part of the kernels  $K_j^{(0)}(\frac{1}{2T} + it)$ . As a result, we get

$$G = \frac{G_C T^2}{24\gamma^2 E_{C,1} E_{C,2}} F_C\left(\frac{\Gamma_1}{T}, \frac{\Gamma_2}{T}\right), \quad (37)$$

where

$$\begin{aligned}
 F_C(p_1, p_2) = & \int_{-\infty}^{\infty} dz \int_{-\infty}^{\infty} du F(p_1, p_2, z, u), \quad (38) \\
 F(p_1, p_2, z, u) = & \frac{p_1 p_2 u [u^2 + 4\pi^2]}{\sinh\left(\frac{u}{2}\right) [\cosh(z) + \cosh\left(\frac{u}{2}\right)]} \\
 & \times \frac{1}{\left[(z + \frac{u}{2})^2 + p_1^2\right] \left[(z - \frac{u}{2})^2 + p_2^2\right]}. \quad (39)
 \end{aligned}$$

The integral in Eq. (6) vanishes due to the particle-hole (PH) symmetry when even in time contribution of both kernels  $K_{1,2}^{(0)}(\frac{1}{2T} \pm it)$  is taken into account. As a result the off-diagonal coefficient  $G_T^{(0)} = 0$ . We therefore need to consider the first nonvanishing correction with respect to the PH-symmetry breaking parameter. By taking into account even-odd products of the kernels  $K_1^{(0)}(\frac{1}{2T} + it)K_2^{(1)}(\frac{1}{2T} - it)$  and  $K_1^{(1)}(\frac{1}{2T} + it)K_2^{(0)}(\frac{1}{2T} - it)$ , we obtain the lowest-order (we consider the model in the vicinity of the intermediate coupling fixed point) nonzero contribution to thermoelectric coefficient as follows:

$$\begin{aligned}
 G_T = & -\frac{G_C T^3}{6e\gamma\pi E_{C,1} E_{C,2}} \\
 & \times \left\{ \frac{|r_1|^2}{\Gamma_1} \ln\left(\frac{E_{C,1}}{T + \Gamma_1}\right) \sin(2\pi N_1) F_{T,s}\left(\frac{\Gamma_1}{T}, \frac{\Gamma_2}{T}\right) \right. \\
 & \left. + \frac{|r_2|^2}{\Gamma_2} \ln\left(\frac{E_{C,2}}{T + \Gamma_2}\right) \sin(2\pi N_2) F_{T,m}\left(\frac{\Gamma_1}{T}, \frac{\Gamma_2}{T}\right) \right\}, \quad (40)
 \end{aligned}$$

where

$$F_{T,s}(p_1, p_2) = \int_{-\infty}^{\infty} dz \int_{-\infty}^{\infty} du \left( z + \frac{u}{2} \right) z F(p_1, p_2, z, u), \quad (41)$$

$$F_{T,m}(p_1, p_2) = \int_{-\infty}^{\infty} dz \int_{-\infty}^{\infty} du \left( z - \frac{u}{2} \right) z F(p_1, p_2, z, u). \quad (42)$$

The Eqs. (37)–(40) represent the central results of this part. By varying parameters such as temperature, gate voltages, and/or reflection amplitudes at the QPCs, one can achieve four different regimes of the thermoelectric transport. The details of the calculations for the electric conductance and the thermal coefficient are represented in the Appendix. We derive and analyze the asymptotic equations for the TP in each regime in four segments below.

### 1. $(\Gamma_1, \Gamma_2) \ll T$ , *non-Fermi-liquid regime*

The TP demonstrates the weak NFL behavior at high temperature:  $T \gg (\Gamma_1, \Gamma_2)$  as

$$S = -\frac{9\gamma}{8e} \left[ |r_1|^2 \ln \left( \frac{E_{C,1}}{T} \right) \sin(2\pi N_1) + |r_2|^2 \ln \left( \frac{E_{C,2}}{T} \right) \sin(2\pi N_2) \right]. \quad (43)$$

The similarity between Eqs. (43) and (28) of Ref. [35] implies that the regime  $T \gg (\Gamma_1, \Gamma_2)$  mimics the perturbative result. The Kondo-resonance width  $\Gamma_j$  vanishes at the Coulomb peaks and increased when the gate voltage  $N_j$  goes out of the half-integer values. This regime is accessible at the center of the  $(N_1, N_2)$  window (if one considers  $0 \leq N_1, N_2 \leq 1$ ). Due to the logarithmic dependence on temperature but small value of TP [see Eq. (43)] we refer to it as a weak NFL scenario.

### 2. $\Gamma_1 \ll T \ll \Gamma_2$ , *non-Fermi-liquid on the left and Fermi liquid on the right CKC*

Let us recall that the Kondo resonances' widths  $\Gamma_1, \Gamma_2$  depend on the gate voltages and therefore represent the energy scales competing with temperature effects in the vicinity of the Coulomb peaks. At the parametric regime  $\Gamma_1 \ll T \ll \Gamma_2$  it corresponds to the domain of the gate voltages such that the QD 1 is fine tuned to a Coulomb peak closer than the QD 2 ( $N_1$  is closer to a half-integer value). The TP consists of two components: weak FL and NFL characteristics as

$$S = -\frac{1024\gamma}{75e\pi^2} \left[ |r_1|^2 \ln \left( \frac{E_{C,1}}{T} \right) \sin(2\pi N_1) + \frac{25\pi^3}{256} |r_2|^2 \frac{T}{\Gamma_2} \ln \left( \frac{E_{C,2}}{\Gamma_2} \right) \sin(2\pi N_2) \right]. \quad (44)$$

The crossover temperature  $T^*$  separating two regimes is defined as

$$\frac{E_{C,2}}{T^*} \ln \left( \frac{E_{C,1}}{T^*} \right) = \frac{25\pi^5}{2048\gamma \cos^2(\pi N_2)} \frac{1}{|r_1|^2} \times \ln \left( \frac{\pi^2}{8\gamma |r_2|^2 \cos^2(\pi N_2)} \right). \quad (45)$$

The NFL behavior dominates if  $T \ll T^*$  while the FL regime is predicted at the opposite limit  $T \gg T^*$ .

### 3. $\Gamma_2 \ll T \ll \Gamma_1$ , *Fermi liquid on the left and non-Fermi-liquid on the right CKC*

This parametric regime is complementary to the case discussed in the Sec. IV B 2. The regime is achieved when the gate voltage applied to the QD 2 tunes it closer to the Coulomb blockade peak than the QD 1 is. The TP is characterized by the weak FL on the left and NFL effect on the right CKC as

$$S = -\frac{1024\gamma}{75e\pi^2} \left[ |r_2|^2 \ln \left( \frac{E_{C,2}}{T} \right) \sin(2\pi N_2) + \frac{25\pi^3}{256} |r_1|^2 \frac{T}{\Gamma_1} \ln \left( \frac{E_{C,1}}{\Gamma_1} \right) \sin(2\pi N_1) \right]. \quad (46)$$

The crossover temperature  $T^{**}$  separating FL and NFL regimes is defined as

$$\frac{E_{C,1}}{T^{**}} \ln \left( \frac{E_{C,2}}{T^{**}} \right) = \frac{25\pi^5}{2048\gamma \cos^2(\pi N_1)} \frac{1}{|r_2|^2} \times \ln \left( \frac{\pi^2}{8\gamma |r_1|^2 \cos^2(\pi N_1)} \right). \quad (47)$$

The NFL behavior dominates when  $T \ll T^{**}$  while the FL regime holds at the opposite limit  $T \gg T^{**}$ . If the two CKCs are identical,  $T^{**} = T^*$ .

### 4. $T \ll (\Gamma_1, \Gamma_2)$ , *Fermi-liquid regime*

In the regime of vanishingly small temperatures  $T \ll (\Gamma_1, \Gamma_2)$  the TP of the system behaves in accordance with the nonperturbative FL scenario:

$$S = -\frac{12\pi\gamma T}{7e} \left[ \frac{|r_1|^2}{\Gamma_1} \ln \left( \frac{E_{C,1}}{\Gamma_1} \right) \sin(2\pi N_1) + \frac{|r_2|^2}{\Gamma_2} \ln \left( \frac{E_{C,2}}{\Gamma_2} \right) \sin(2\pi N_2) \right]. \quad (48)$$

On the one hand, the TP is a linear function of the temperature, which is the hallmark for the FL regime. On the other hand, the prefactors are giant when both QDs are fine tuned by the gate voltages to the regime of the vicinities of the Coulomb peaks. The system therefore is characterized by FL properties strongly renormalized by the scattering and interactions.

The advantage of the nonperturbative solution in comparison to the perturbative one is that the latter is applicable only to the temperature regime  $|r_j|^2 E_{C,j} \ll T \ll E_{C,j}$  while the former can be used at any small temperature. With the appearance of the two Kondo resonance width energy scales  $\Gamma_1, \Gamma_2$  in the nonperturbative treatment, we can identify four different limit regimes as represented above. They correspond to four regimes shown in Fig. 3, left panel, as: the first: red; the second: blue; the third: yellow; and the fourth: green. The right panel of Fig. 3 represents the contour plot of thermopower as a function of  $(N_1, N_2)$ . The perturbative result belongs to the first regime  $(\Gamma_1, \Gamma_2) \ll T$  in which the temperature scaling of

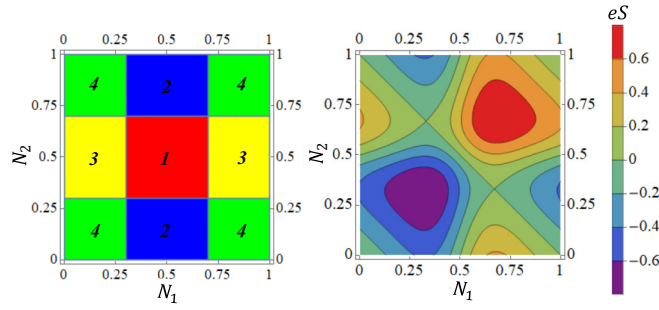


FIG. 3. Left panel: Region plot of four segments (the number marked on each one corresponds to the regime in the main text) as functions of the dimensionless gate voltages  $N_1$  and  $N_2$ . 1 - red region:  $\Gamma_1, \Gamma_2 \leq T$ , 2 - blue region:  $\Gamma_1 \leq T < \Gamma_2$ , 3 - yellow region:  $\Gamma_2 \leq T < \Gamma_1$ , 4 - green region:  $T < \Gamma_1, \Gamma_2$ . Right panel: Contour plot of thermopower as function of the dimensionless gate voltages  $N_1$  and  $N_2$  computed from general formula. Other parameters:  $|r_1|^2 = 0.1, |r_2|^2 = 0.1, T/E_C = 0.05$  ( $E_{C,1} = E_{C,2} = E_C$ ).

TP behaves in accordance with the NFL scenario. Thanks to the NFL enhancement of the heat proliferation the TP reaches the biggest value when  $(\Gamma_1, \Gamma_2) \rightarrow T$  at low-temperature regime (see also in Fig. 4).

Depending on a domain of external parameters the TP of the 2SCKC behaves in accordance with either NFL or FL scenario. TP is a subject to one of the four regimes shown in Fig. 3, left panel, when the temperature is varied. Behavior of the TP maximum computed from the general formulas [see Eqs. (37) and (40)] as a function of temperature for the different sets of reflection amplitudes:  $|r_1|^2 = |r_2|^2 = 0.1$  (continuous line) and  $|r_1|^2 = 0.1, |r_2|^2 = 0.08$  (dashed line) is shown on in Fig. 4(a). In Figs. 4(b) and 4(c) we investigate these cases in detail. Namely, the maximum of TP taken from general formulas and Eq. (43) (perturbative solution) are plotted by the blue and red lines at the same dimensionless gate voltages  $(N_{10}, N_{20})$ , respectively. Besides, in Figs. 4(b) and 4(c), the maximums of TP  $eS_{\max}$  are plotted as functions of the ratio  $T/T_{\text{per}}$  where  $T_{\text{per}}$  is defined as  $T_{\text{per}} = \max[|r_j|^2]E_C$ . Thus,  $T_{\text{per}} = 0.1$  in both panels. Clearly, the perturbative solution of the first regime ( $\Gamma_1, \Gamma_2 \ll T$ ) is achieved on the right side of the point at  $T/T_{\text{per}} = O(1)$ . Figure 5 provides more details on the validity regime of the perturbative solution. Namely, the condition  $T_{\text{per}} \ll T \ll E_C$  can be adapted only when  $|r_j|$  are small enough [38].

On Figs. 4(b) and 4(c) we show by black lines the temperature behavior of the TP computed at specific values of dimensionless gate voltages  $N_{11}$  and  $N_{21}$  satisfying conditions  $\Gamma_1(N_{11}) = T$  and  $\Gamma_2(N_{21}) = T$ . Remarkably, the regimes where TP gets maximum value, are at  $(\Gamma_1, \Gamma_2) \sim T$ . On the one hand,  $(\Gamma_1, \Gamma_2) > T$  at very low temperatures (the left side of the crossing point between the blue and black lines). On the other hand,  $(\Gamma_1, \Gamma_2) < T$  at higher temperatures (the right side of the crossing point). We conclude that to observe the fingerprints of the NFL behavior in the thermoelectric transport of the 2SCKCs it is sufficient to perform several sets of experiments at different temperatures from the highest one  $T \gg |r_j|^2 E_{C,j}$  to the lowest possible (notice that the temperature is anyway bounded from below by the mean level spacing

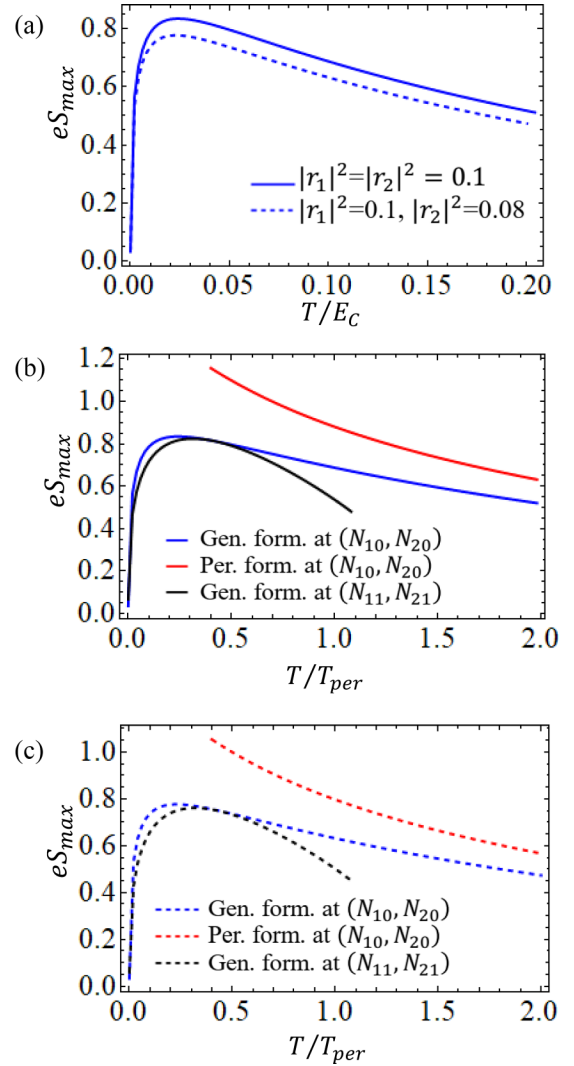


FIG. 4. Maximum of thermopower as a function of temperature. The value  $eS_{\max}$  is achieved at  $(N_{10}, N_{20})$ . (a) the curves for plots are computed using general formulas [see Eqs. (35) and (38)] for different sets of reflection amplitudes:  $|r_1|^2 = |r_2|^2 = 0.1$  (continuous line) and  $|r_1|^2 = 0.1, |r_2|^2 = 0.08$  (dashed line). (b) and (c)  $eS_{\max}$  as a function of  $T/T_{\text{per}}$  ( $T_{\text{per}} = \max[|r_j|^2]E_C = 0.1$  in both panels) are plot for these two parameter sets: blue lines are maximum of thermopower  $eS_{\max}$  taken from general formulas, red lines describe the thermopower computed from Eq. (43) (perturbative solution) at  $(N_{10}, N_{20})$ , while black lines correspond to the thermopower computed at the gate voltages  $(N_{11}, N_{21})$  at which  $\Gamma_1(N_{11}) = T$  and  $\Gamma_2(N_{21}) = T$  ( $E_{C,1} = E_{C,2} = E_C$ ). The perturbative calculation's validity is defined by the condition  $T/T_{\text{per}} = 1$  fulfilled on the right side of the plots.

of the QD being the smallest energy parameter of the model). Besides, the condition of the vicinity to the Coulomb peaks provides an access to crossing three distinct regimes: either  $(1 \rightarrow 2 \rightarrow 4)$  or  $(1 \rightarrow 3 \rightarrow 4)$  where the crossover between NFL and FL behavior is predicted to be pronounced (here digits  $n = 1 \rightarrow 4$  refer to four distinct temperature regimes discussed in Sec. IV and analyzed in gross detail in subsections. Necessary details of calculations are presented in the Appendix.)

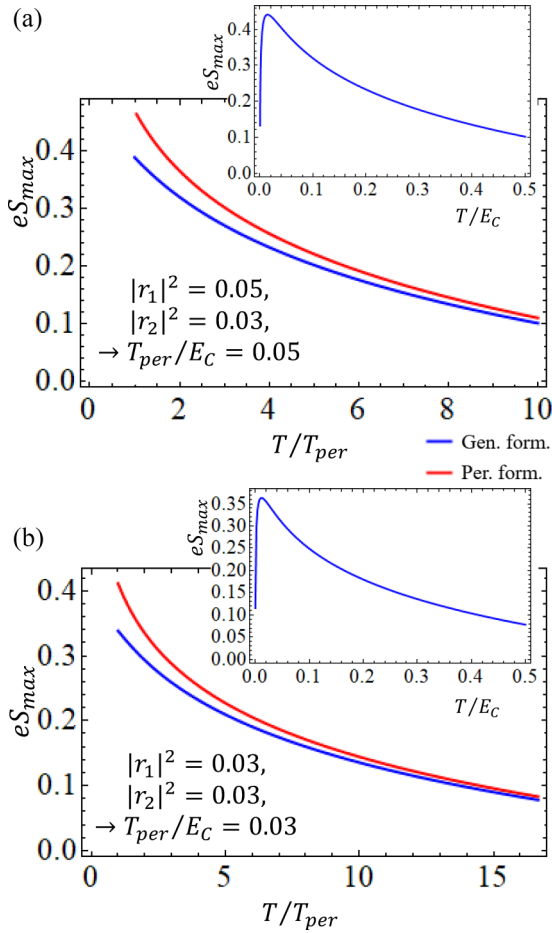


FIG. 5. Maximum of thermopower  $eS_{\max}$  as a function of  $T/T_{\text{per}}$ . Blue and red lines are computed from the general formulas and perturbation approach, respectively. (a)  $|r_1|^2 = 0.05$ ,  $|r_2|^2 = 0.03$ , so  $T_{\text{per}}/E_C = 0.05$  and (b)  $|r_1|^2 = |r_2|^2 = 0.03$ , so  $T_{\text{per}}/E_C = 0.03$ . The inserts: Maximum of thermopower as a function of temperature. The perturbative result approaches the general one when  $T/T_{\text{per}} \gg 1$  ( $E_{C,1} = E_{C,2} = E_C$ ).

## V. DISCUSSION AND CONCLUSION

The investigation of TP for the weak coupling between two CKCs in both cases: 1CK-2CK and 2CK-2CK shows the competition between the FL and NFL picture. However, the windows of parameters to observe the FL property are much broader than the windows to access the NFL one. The reason is that the NFL intermediate coupling fixed points of MCK are hyperbolic and therefore unstable. The results of this work not only cover the perturbative accessible regimes, which have been represented in Ref. [35], but also show a rich property of the TP in different domains of parameters.

*Figure of merit ZT.* In order to estimate the figure of merit ZT in the 2SCKCs we rewrite the Eq (10) in the following form:

$$ZT = \frac{S^2}{L_0 \cdot R(T)}, \quad \frac{\mathcal{K}}{GT} = L_0 \cdot R(T) = L_0 \cdot R_L - S^2. \quad (49)$$

On the one hand, the ZT is proportional to the second power of the TP. On the other hand, it is inversely proportional to the Lorenz ratio  $R_L$  [39]. The conventional WF law predicts  $R_L = 1$  at  $T = 0$  with vanishingly small corrections at low temperatures. The generalized WF law discussed in Ref. [39] says that the Lorenz ratio in the 2SCKCs is in general greater than unity and in particular, bounded from above by the value  $R_L^{\max} = 27/7$ . Therefore, two competing effects take place: the NFL scenario significantly enhances the thermoelectric power at low temperatures compare to the FL value while Anderson orthogonality catastrophe results in increase of the Lorenz ratio [39]. Yet another bad news for the figure of merit are associated with vanishing of TP at the low-temperature regime and vanishing of TP for the almost transparent QPC setups (small reflection amplitude is a PH breaking parameter, which has to be controllable small for the validity of the whole theory). As one can see it from Figs. 4 and 5, the maximum of TP is reached at the crossover temperature regime  $(\Gamma_1, \Gamma_2) \approx T$  at the very vicinity of the Coulomb peaks  $N_j \approx 0.5 \pm \delta N_j$ . Following Matveev-Andreev [24] we estimate  $\delta N_j \sim 1/|r_j| \sqrt{T/E_{C,j}}$ . It finally results in the best ZT estimate

$$[ZT]_{\max} \rightarrow \frac{a}{R_L} |r|^2 \frac{\Gamma}{E_C} \ln^2 \left( \frac{E_C}{\Gamma} \right) \quad (50)$$

with  $a \lesssim 1$ . For this estimation we choose  $|r_1| = |r_2| = |r|$ ,  $\Gamma_1 = \Gamma_2 = \Gamma$  and  $E_{C,1} = E_{C,2} = E_C$ . For realistic 2SCKCs  $[ZT]_{\max} \sim |r|^4 \ln^2(|r|^2) \ll 1$ .

Extending the proposal of the weak coupling between two CKCs [35] to the regime of almost transparent QPC in the central area of the 2SCKC, the very recent experiment [69] and theory [70,71] have investigated the strong coupling limit. Let us comment on the connection between the weak and strong coupling regimes of the 2SCKCs. In Ref. [35] we have considered the 2SCKC weakly connecting 1CK-1CK or 1CK-2CK or 2CK-2CK. The same realization for the strong coupling of two Kondo simulators has also been theoretically suggested in Ref. [35] and experimentally realized recently in Ref. [69] for 1CK-1CK coupling [79]. One of the most exciting theoretical predictions of the two-impurity single-channel Kondo effect [81–83] is a possibility to map the model under certain assumptions onto the 2CK Hamiltonian. Interestingly, the Refs. [69–71] showed that at the triple degeneracy point of the 2SCKC  $Z_3$  symmetry and corresponding local parafermion emerge. It is straightforward to extend the idea [35] to MCK-NCK strong coupling (see Fig. 6). Suppose that there are  $M > 1$  identical QPCs in the left-hand side of the 2SCKC and  $N > 1$  identical QPCs in the right side of it. The total degeneracy is  $M + 1 + N$  and corresponding emergent local symmetry is  $Z_{M+N+1}$ . There are three important  $(M, N)$  realizations accessible through existing experimental setups: (i) (2,1) or (1,2) connecting 1CK and 2CK with emergent symmetry  $Z_4$ ; (ii) (2,2); and (iii) (3,1) or (1,3) with emergent symmetry  $Z_5$ . Corresponding weak link setups are characterized by the symmetries: (i)  $U(1) \times Z_2$ ; (ii)  $Z_2 \times Z_2$ ; and (iii)  $U(1) \times Z_3$ . As the weak coupling regimes of (ii) and (iii) are clearly distinct, being characterized by both different symmetries and different Lorenz ratios (see Ref. [39] for more details), it is interesting to examine regimes (ii) and (iii) in the strong coupling limit. In particular it is important to

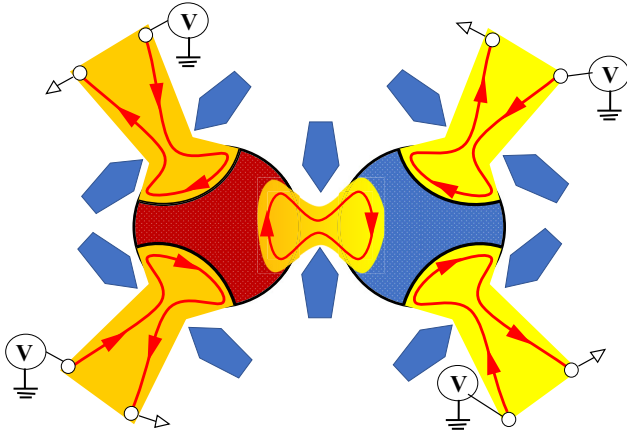


FIG. 6. Schematic of a strong coupling between two charge Kondo circuits. Notations are the same as on Fig. 1 with two distinct differences: (i) different color scheme used for the left (orange, hot) and right (yellow, cold) parts of the circuit; (ii) the central part of the system is modified. The tunnel contact in the center of Fig. 1 is replaced by almost transparent QPC. The chiral edge mode strongly couples QD1 and QD2. The temperature gradient (shown by continuous change of color from orange to yellow) is applied across the central QPC.

understand the symmetry of local parafermion emerging in the strong link setup. In addition, switching between different intermediate coupling fixed points results in crossovers between various fractionalized modes manifesting itself in distinctly different regimes of the charge and heat transport.

The weak link regime discussed in this paper was analyzed using a standard approach based on the transport integrals [35]. The validity of this approach is justified by an assumption that both temperature and voltage drops occur exactly at the central tunnel barrier. As a result, both the left and the right parts of the 2SCKC are considered at thermal and mechanical equilibrium being characterized by certain temperature  $T$  and chemical potential  $\mu$ . This approach is clearly invalid for the strong link between two sides of the Kondo simulator where both the temperature and the voltage changes continuously across the central QPC. The full-fledged linear response theory of the charge and heat transport across the strong link of the two-site Kondo simulators can be constructed by using Luttinger's pseudogravitational approach [84,85] or thermo-mechanical potential [86,87] method in combination with Kubo equations. The theory beyond linear response requires also using Keldysh formalism [86,87] and represents an interesting and important direction for the future investigation.

In summary, we revisited the thermoelectric transport at the weak link of the 2SCKC model proposed in the Ref. [35]. The Abelian bosonization approach is used for both 1CK and 2CK setup while the refermionization technique is applied in order to solve the 2CK model nonperturbatively. We show the different windows of the parameter set where the temperature dependence of TP behaves either the full FL or NFL characteristics or the competition between these properties. The nonperturbative results not only cover the perturbative results but also be applicable in the lower-temperature regime  $T < |r_j|^2 E_{C,j}$ . We predict that the TP is enhanced in the

2SCKC in comparison with the single CKC setup. Indeed, complex charge Kondo circuits showing the diversity of the competition between the FL and NFL properties represent new classes of the quantum simulators characterized by a significant improvement of the thermoelectric properties. The models describing the charge and heat transport through these devices deserve extensive theoretical and experimental studies in the future. The realistic figures of merit of the 2SCKCs are, however, still far from approaching the numbers demanded by the quantum computer applications. Detailed investigation of the multisite quantum simulators in the NFL operational regimes provides a promising avenue for the new quantum technologies. Finally, we propose to use the experimental implementation in Ref. [69] for investigating the different parafermion contributions to the quantum thermoelectricity when the coupling between QDs is switched from weak to strong.

## ACKNOWLEDGMENTS

This research in Hanoi is funded by Vietnam Academy of Science and Technology (program for Physics development) under Grant No. KHCBVL.06/23-24. The work of M.N.K is conducted within the framework of the Trieste Institute for Theoretical Quantum Technologies (TQT). M.N.K also acknowledges the support from the Alexander von Humboldt Foundation for the research visit to IFW Dresden. The research of M.N.K. was supported in part by the National Science Foundation under Grants No. NSF PHY-1748958 and No. PHY-2309135. M.N.K. acknowledges support of the Institute Henri Poincaré (UAR 839 CNRS-Sorbonne Université) and LabEx CARMIN (ANR-10LABX-59-01).

## APPENDIX

In this Appendix we represent the details of the different approaches at different limits in order to obtain the results shown in the Sec. IV B.

(1) If  $p_1 \rightarrow 0$ ,  $p_2 \rightarrow 0$ , we have:

$$\lim_{p_1 \rightarrow 0} \frac{p_1}{\left(z + \frac{u}{2}\right)^2 + p_1^2} = \pi \delta\left(z + \frac{u}{2}\right), \quad (\text{A1})$$

$$\lim_{p_2 \rightarrow 0} \frac{p_2}{\left(z - \frac{u}{2}\right)^2 + p_2^2} = \pi \delta\left(z - \frac{u}{2}\right). \quad (\text{A2})$$

As a result

$$\begin{aligned} \lim_{p_2 \rightarrow 0} \frac{F_{T,m}(p_1 \rightarrow 0, p_2)}{p_2} &= \lim_{p_2 \rightarrow 0} \int_{-\infty}^{\infty} du \frac{\pi u^3 [u^2 + 4\pi^2]}{2 \sinh[u] [u^2 + p_2^2]} \\ &= \int_{-\infty}^{\infty} du \frac{\pi u [u^2 + 4\pi^2]}{2 \sinh[u]} = \frac{9\pi^5}{8}, \end{aligned} \quad (\text{A3})$$

and, finally

$$\lim_{p_1 \rightarrow 0} \frac{F_{T,s}(p_1, p_2 \rightarrow 0)}{p_1} = \frac{9\pi^5}{8}. \quad (\text{A4})$$

We obtain the electric conductance as

$$G = \frac{\pi^4 G_C T^2}{6\gamma^2 E_{C,1} E_{C,2}}, \quad (\text{A5})$$

and the thermoelectric coefficient as

$$G_T = -\frac{3\pi^4 G_C T^2}{16e\gamma E_{C,1} E_{C,2}} \left[ |r_1|^2 \ln\left(\frac{E_{C,1}}{T}\right) \sin(2\pi N_1) + |r_2|^2 \ln\left(\frac{E_{C,2}}{T}\right) \sin(2\pi N_2) \right]. \quad (\text{A6})$$

(2) If  $p_1 \rightarrow 0$ ,  $p_2 \gg 1$  we have:

$$F_C(p_1 \rightarrow 0, p_2) = \int_{-\infty}^{\infty} du \frac{\pi p_2 u [u^2 + 4\pi^2]}{\sinh[u] [u^2 + p_2^2]},$$

$$F_C(p_1 \rightarrow 0, p_2 \gg 1) = \frac{\pi}{p_2} \int_{-\infty}^{\infty} du \frac{u [u^2 + 4\pi^2]}{\sinh[u]} = \frac{9\pi^5}{4p_2}, \quad (\text{A7})$$

and

$$F_{T,m}(p_1 \rightarrow 0, p_2 \gg 1) = \frac{\pi}{2p_2} \int_{-\infty}^{\infty} du \frac{u^3 [u^2 + 4\pi^2]}{\sinh[u]} = \frac{3\pi^7}{4p_2}. \quad (\text{A8})$$

The calculation of the  $F_{T,s}$  is a bit complicated, which concerns the principal value (PV) as follows.

$$\begin{aligned} \frac{F_{T,s}(p_1 \rightarrow 0, p_2 \gg 1)}{p_1} &= \frac{1}{p_2} \text{PV} \int_{-\infty}^{\infty} dz \int_{-\infty}^{\infty} du \frac{uz [u^2 + 4\pi^2]}{(z + \frac{u}{2}) \sinh(\frac{u}{2}) [\cosh(z) + \cosh(\frac{u}{2})]} \\ &= \frac{8}{p_2} \int_{-\infty}^{\infty} dp \int_{-\infty}^{\infty} dq \left\{ \frac{q [q^2 + \pi^2]}{\sinh(q) \cosh(p/2) \cosh(p/2 - q)} - \frac{\tanh(p/2) q^2 [q^2 + \pi^2]}{p \cosh(p/2 + q) \cosh(p/2 - q)} \right\} \\ &= \frac{192\pi^4}{25p_2}. \end{aligned} \quad (\text{A9})$$

The electric conductance  $G$  and the thermoelectric coefficient  $G_T$  is computed at the first nonzero term in the nonperturbative treatment are

$$G = \frac{3G_C \pi^5 T^3}{32\gamma^2 \Gamma_2 E_{C,1} E_{C,2}}, \quad (\text{A10})$$

$$G_T = -\frac{32G_C \pi^3 T^3}{25e\gamma E_{C,1} E_{C,2} \Gamma_2} \left[ |r_1|^2 \ln\left(\frac{E_{C,1}}{T}\right) \sin(2\pi N_1) + \frac{25\pi^3}{256} |r_2|^2 \frac{T}{\Gamma_2} \ln\left(\frac{E_{C,2}}{\Gamma_2}\right) \sin(2\pi N_2) \right]. \quad (\text{A11})$$

(3)  $p_1 \gg 1$ ,  $p_2 \rightarrow 0$ : This limit is opposite to the second limit. The calculation process is the same as the above one.

$$F_C(p_1 \gg 1, p_2 \rightarrow 0) = \frac{\pi}{p_1} \int_{-\infty}^{\infty} du \frac{u [u^2 + 4\pi^2]}{\sinh[u]} = \frac{9\pi^5}{4p_1}, \quad (\text{A12})$$

$$\begin{aligned} \frac{F_{T,m}(p_1 \gg 1, p_2 \rightarrow 0)}{p_2} &= \frac{1}{p_1} \text{PV} \int_{-\infty}^{\infty} dz \int_{-\infty}^{\infty} du \frac{uz [u^2 + 4\pi^2]}{(z - \frac{u}{2}) \sinh(\frac{u}{2}) [\cosh(z) + \cosh(\frac{u}{2})]} \\ &= \frac{192\pi^4}{25p_1}, \end{aligned} \quad (\text{A13})$$

$$F_{T,s}(p_1 \gg 1, p_2 \rightarrow 0) = \frac{3\pi^7}{4p_1}. \quad (\text{A14})$$

The electric conductance is

$$G = \frac{3G_C \pi^5 T^3}{32\gamma^2 E_{C,1} E_{C,2} \Gamma_1}, \quad (\text{A15})$$

and the thermoelectric coefficient is

$$G_T = -\frac{32G_C \pi^3 T^3}{25e\gamma E_{C,1} E_{C,2} \Gamma_1} \left[ |r_2|^2 \ln\left(\frac{E_{C,2}}{T}\right) \sin(2\pi N_2) + \frac{25\pi^3}{256} |r_1|^2 \frac{T}{\Gamma_1} \ln\left(\frac{E_{C,1}}{\Gamma_1}\right) \sin(2\pi N_1) \right]. \quad (\text{A16})$$

(4) If  $p_1 \gg 1$ ,  $p_2 \gg 1$ , we simply remove the terms, which are summed with  $p_1^2$  and  $p_2^2$  in the denominator of the formula (39). We then obtain:

$$F_C(p_1 \gg 1, p_2 \gg 1) = \frac{1}{p_1 p_2} \int_{-\infty}^{\infty} dz \int_{-\infty}^{\infty} du \frac{u[u^2 + 4\pi^2]}{\sinh\left[\frac{u}{2}\right][\cosh(z) + \cosh\left(\frac{u}{2}\right)]} = \frac{64\pi^4}{5p_1 p_2}. \quad (\text{A17})$$

$$F_{T,m}(p_1 \gg 1, p_2 \gg 1) = \frac{1}{p_1 p_2} \int_{-\infty}^{\infty} dz \int_{-\infty}^{\infty} du \frac{(z - \frac{u}{2})uz[u^2 + 4\pi^2]}{\sinh\left[\frac{u}{2}\right][\cosh(z) + \cosh\left(\frac{u}{2}\right)]} = \frac{192\pi^6}{35p_1 p_2}. \quad (\text{A18})$$

$$F_{T,s}(p_1 \gg 1, p_2 \gg 1) = \frac{1}{p_1 p_2} \int_{-\infty}^{\infty} dz \int_{-\infty}^{\infty} du \frac{(z + \frac{u}{2})uz[u^2 + 4\pi^2]}{\sinh\left[\frac{u}{2}\right][\cosh(z) + \cosh\left(\frac{u}{2}\right)]} = \frac{192\pi^6}{35p_1 p_2}. \quad (\text{A19})$$

The electric conductance and the thermoelectric coefficient in this limit are

$$G = \frac{8G_C \pi^4 T^4}{15\gamma^2 E_{C,1} E_{C,2} \Gamma_1 \Gamma_2}, \quad (\text{A20})$$

$$G_T = -\frac{32G_C \pi^5 T^5}{35e\gamma E_{C,1} E_{C,2} \Gamma_1 \Gamma_2} \left\{ \frac{|r_1|^2}{\Gamma_1} \ln\left(\frac{E_{C,1}}{T + \Gamma_1}\right) \sin(2\pi N_1) + \frac{|r_2|^2}{\Gamma_2} \ln\left(\frac{E_{C,2}}{T + \Gamma_2}\right) \sin(2\pi N_2) \right\}. \quad (\text{A21})$$

- 
- [1] G. Snyder and E. Toberer, Complex thermoelectric materials, *Nat. Mater.* **7**, 105 (2008).
- [2] T. J. Seebeck, Über den Magnetismus der galvanischen Kette, *Abh. preuss. Akad. Wiss.* **1820**, 289 (1822); Magnetische Polarisation der Metalle und Erze durch Temperatur-Differenz, 265 (1825).
- [3] J. F. Li, W. S. Liu, L. D. Zhao, and M. Zhou, High-performance nanostructured thermoelectric materials, *NPG Asia Mater.* **2**, 152 (2010).
- [4] Y. Du, K. F. Cai, S. Chen, H. Wang, S. Z. Shen, R. Donelson, and T. Lin, Thermoelectric fabrics: toward power generating clothing, *Sci. Rep.* **5**, 6144 (2015).
- [5] L. D. Hicks and M. S. Dresselhaus, *Phys. Rev. B* **47**, 12727 (1993); Thermoelectric figure of merit of a one-dimensional conductor, **47**, 16631(R) (1993).
- [6] G. D. Mahan and J. O. Sofo, The best thermoelectric, *Proc. Natl. Acad. Sci. USA* **93**, 7436 (1996).
- [7] M. S. Dresselhaus, G. Chen, M. Y. Tang, R. G. Yang, H. Lee, D. Z. Wang, Z. F. Ren, J. P. Fleurial, P. Gogna, New directions for low-dimensional thermoelectric materials, *Adv. Mater.* **19**, 1043 (2007).
- [8] G. Chen, M. S. Dresselhaus, G. Dresselhaus, J. P. Fleurial, and T. Caillat, Recent developments in thermoelectric materials, *Int. Mater. Rev.* **48**, 45 (2003).
- [9] A. I. Hochbaum, R. Chen, R. D. Delgado, W. Liang, E. C. Garnett, M. Najarian, A. Majumdar, and P. Yang, Enhanced thermoelectric performance of rough silicon nanowires, *Nature (London)* **451**, 163 (2008); A. I. Boukai, Y. Bunimovich, J. Tahir-Kheli, J.-K. Yu, W. A. Goddard III, and J. R. Heath, Silicon nanowires as efficient thermoelectric materials, *ibid.* **451**, 168 (2008).
- [10] Y. M. Blanter and Y. V. Nazarov, *Quantum Transport: Introduction to Nanoscience* (Cambridge University Press, Cambridge, 2009).
- [11] K. Kikoin, M. N. Kiselev, and Y. Avishai, *Dynamical Symmetry for Nanostructures. Implicit Symmetry in Single-Electron Transport Through Real and Artificial Molecules* (Springer, New York, 2012).
- [12] A. A. M. Staring, L. W. Molenkamp, B. W. Alphenhaar, H. van Houten, O. J. A. Buyk, M. A. A. Mabeesoone, C. W. J. Beenakker, and C. T. Foxon, Coulomb-blockade oscillations in the thermopower of a quantum dot, *Europhys. Lett.* **22**, 57 (1993).
- [13] M. Turek and K. A. Matveev, Cotunneling thermopower of single electron transistors, *Phys. Rev. B* **65**, 115332 (2002).
- [14] M. Krawiec and K. I. Wysokiński, Thermoelectric effects in strongly interacting quantum dot coupled to ferromagnetic leads, *Phys. Rev. B* **73**, 075307 (2006).
- [15] T. A. Costi and V. Zlatić, Thermoelectric transport through strongly correlated quantum dots, *Phys. Rev. B* **81**, 235127 (2010).
- [16] P. Trocha and J. Barnaś, Large enhancement of thermoelectric effects in a double quantum dot system due to interference and Coulomb correlation phenomena, *Phys. Rev. B* **85**, 085408 (2012).
- [17] S. Donsa, S. Andergassen, and K. Held, Double quantum dot as a minimal thermoelectric generator, *Phys. Rev. B* **89**, 125103 (2014).
- [18] K. P. Wójcik and I. Weymann, Thermopower of strongly correlated T-shaped double quantum dots, *Phys. Rev. B* **93**, 085428 (2016).
- [19] A. Svilans, M. Josefsson, A. M. Burke, S. Fahlvik, C. Thelander, H. Linke, and M. Leijnse, Thermoelectric characterization of the Kondo resonance in nanowire quantum dots, *Phys. Rev. Lett.* **121**, 206801 (2018).
- [20] B. Dutta, D. Majidi, A. G. Corral, P. A. Erdman, S. Florens, T. A. Costi, H. Courtois, and C. B. Winkelmann, Direct probe of the seebeck coefficient in a

- Kondo-correlated single-quantum-dot transistor, *Nano Lett.* **19**, 506 (2019).
- [21] K. Flensberg, Capacitance and conductance of mesoscopic systems connected by quantum point contacts, *Phys. Rev. B* **48**, 11156 (1993).
- [22] K. A. Matveev, Coulomb blockade at almost perfect transmission, *Phys. Rev. B* **51**, 1743 (1995).
- [23] A. Furusaki and K. A. Matveev, Coulomb blockade oscillations of conductance in the regime of strong tunneling, *Phys. Rev. Lett.* **75**, 709 (1995).
- [24] K. A. Matveev and A. V. Andreev, Coulomb blockade oscillations in the thermopower of open quantum dots *Phys. Rev. Lett.* **86**, 280 (2001); Thermopower of a single-electron transistor in the regime of strong inelastic cotunneling, *Phys. Rev. B* **66**, 045301 (2002).
- [25] K. Le Hur, Zeeman smearing of the Coulomb blockade, *Phys. Rev. B* **64**, 161302(R) (2001).
- [26] K. Le Hur and G. Seelig, Capacitance of a quantum dot from the channel-anisotropic two-channel Kondo model, *Phys. Rev. B* **65**, 165338 (2002).
- [27] J. Kondo, Resistance minimum in dilute magnetic alloys, *Prog. Theor. Phys.* **32**, 37 (1964).
- [28] A. Hewson, *The Kondo Problem to Heavy Fermions* (Cambridge University Press, Cambridge, 1993).
- [29] A. M. Tselik and P. B. Wiegmann, Exact results in the theory of magnetic alloys, *Adv. Phys.* **32**, 453 (1983).
- [30] N. Andrei, K. Furuya, and J. H. Lowenstein, Solution of the Kondo problem, *Rev. Mod. Phys.* **55**, 331 (1983).
- [31] L. Kouwenhoven and L. I. Glazman, Revival of the Kondo effect, *Phys. World* **14**, 33 (2001).
- [32] R. Scheibner, H. Buhmann, D. Reuter, M. N. Kiselev, and L. W. Molenkamp, Thermopower of a Kondo spin-correlated quantum dot, *Phys. Rev. Lett.* **95**, 176602 (2005).
- [33] T. K. T. Nguyen, M. N. Kiselev, and V. E. Kravtsov, Thermoelectric transport through a quantum dot: Effects of asymmetry in Kondo channels, *Phys. Rev. B* **82**, 113306 (2010).
- [34] T. K. T. Nguyen and M. N. Kiselev, Protection of a non-Fermi liquid by spin-orbit interaction, *Phys. Rev. B* **92**, 045125 (2015).
- [35] T. K. T. Nguyen and M. N. Kiselev, Seebeck effect on a weak link between Fermi and non-Fermi liquids, *Phys. Rev. B* **97**, 085403 (2018).
- [36] A. V. Parafilo, T. K. T. Nguyen, and M. N. Kiselev, Thermoelectrics of a two-channel charge Kondo circuit: Role of electron-electron interactions in a quantum point contact, *Phys. Rev. B* **105**, L121405 (2022).
- [37] A. V. Parafilo and T. K. T. Nguyen, Thermopower of a Luttinger-liquid-based two-channel charge Kondo circuit: non-perturbative solution, *Commun. Phys.* **33**, 1 (2023).
- [38] T. K. T. Nguyen and M. N. Kiselev, Heat conductance oscillations in two weakly connected charge Kondo circuits, *Commun. Phys.* **32**, 331 (2022).
- [39] M. N. Kiselev, Generalized Wiedemann-Franz law in a two-site charge Kondo circuit: Lorenz ratio as a manifestation of the orthogonality catastrophe, *Phys. Rev. B* **108**, L081108 (2023).
- [40] T. K. T. Nguyen and M. N. Kiselev, Quantum transport through a “charge” Kondo circuit: Effects of weak repulsive interaction in Luttinger liquid, *Commun. Phys.* **30**, 1 (2020).
- [41] T. K. T. Nguyen, A. V. Parafilo, H. Q. Nguyen, and M. N. Kiselev, Charge Kondo circuit as a detector for electron-electron interactions in a Luttinger liquid, *Phys. Rev. B* **107**, L201402 (2023).
- [42] A. V. Parafilo, V. M. Kovalev, and I. G. Savenko, Probing Luttinger liquid properties in a multichannel two-site charge Kondo simulator, *Phys. Rev. B* **108**, L201101 (2023).
- [43] E. Sela, A. K. Mitchell, and L. Fritz, Exact crossover green function in the two-channel and two-impurity Kondo models, *Phys. Rev. Lett.* **106**, 147202 (2011).
- [44] A. K. Mitchell, L. A. Landau, L. Fritz, and E. Sela, Universality and scaling in a charge two-channel Kondo device, *Phys. Rev. Lett.* **116**, 157202 (2016).
- [45] L. A. Landau, E. Cornfeld, and E. Sela, Charge fractionalization in the two-channel Kondo effect, *Phys. Rev. Lett.* **120**, 186801 (2018).
- [46] G. A. R. van Dalum, A. K. Mitchell, and L. Fritz, Wiedemann-Franz law in a non-Fermi liquid and Majorana central charge: Thermoelectric transport in a two-channel Kondo system, *Phys. Rev. B* **102**, 041111(R) (2020).
- [47] R. Shinzaki, J. Nasu, and A. Koga, Charge Kondo effect and superconductivity in the Falikov-Kimball model with pair hopping, *Phys. Rev. B* **97**, 125130 (2018).
- [48] P. Werner and A. J. Millis, Hybridization expansion impurity solver: General formulation and application to Kondo lattice and two-orbital models, *Phys. Rev. B* **74**, 155107 (2006).
- [49] E. Gull, A. J. Millis, A. I. Lichtenstein, A. N. Rubtsov, M. Troyer, and P. Werner, Continuous-time Monte Carlo methods for quantum impurity models, *Rev. Mod. Phys.* **83**, 349 (2011).
- [50] C. Bertrand, O. Parcollet, A. Maillard, and X. Waintal, Quantum Monte Carlo algorithm for out-of-equilibrium Green’s functions at long times, *Phys. Rev. B* **100**, 125129 (2019).
- [51] M. Maček, P. T. Dumitrescu, C. Bertrand, B. Triggs, O. Parcollet, and X. Waintal, Quantum quasi-Monte Carlo technique for many-body perturbative expansions, *Phys. Rev. Lett.* **125**, 047702 (2020).
- [52] Z. Iftikhar, S. Jezouin, A. Anthore, U. Gennser, F. D. Parmentier, A. Cavanna, and F. Pierre, Two-channel Kondo effect and renormalization flow with macroscopic quantum charge states, *Nature (London)* **526**, 233 (2015).
- [53] Z. Iftikhar, A. Anthore, A. K. Mitchell, F. D. Parmentier, U. Gennser, A. Ouerghi, A. Cavanna, C. Mora, P. Simon, and F. Pierre, Tunable quantum criticality and super-ballistic transport in a “charge” Kondo circuit, *Science* **360**, 1315 (2018).
- [54] Ph. Nozières and A. Blandin, Kondo effect in real metals, *J. Phys.* **41**, 193 (1980).
- [55] D. Cox and A. Zawadowski, Exotic Kondo effects in metals: Magnetic ions in a crystalline electric field and tunnelling centres, *Adv. Phys.* **47**, 599 (1998).
- [56] I. Affleck and A. W. W. Ludwig, Exact conformal-field-theory results on the multichannel Kondo effect: Single-fermion Green’s function, self-energy, and resistivity, *Phys. Rev. B* **48**, 7297 (1993).
- [57] N. Andrei and C. Destri, Solution of the multichannel Kondo problem, *Phys. Rev. Lett.* **52**, 364 (1984).
- [58] M. Fabrizio, A. O. Gogolin, and P. Nozières, Crossover from non-fermi-liquid to fermi-liquid behavior in the two channel Kondo model with channel anisotropy, *Phys. Rev. Lett.* **74**, 4503 (1995).
- [59] M. Fabrizio, A. O. Gogolin, and P. Nozières, Anderson-Yuval approach to the multichannel Kondo problem, *Phys. Rev. B* **51**, 16088 (1995).

- [60] A. O. Gogolin, A. A. Nersisyan, and A. M. Tsvelik, *Bosonization Approach to Strongly Correlated Systems* (Cambridge University Press, Cambridge, 1998).
- [61] V. J. Emery and S. Kivelson, Mapping of the two-channel Kondo problem to a resonant-level model, *Phys. Rev. B* **46**, 10812 (1992).
- [62] A. B. Zamolodchikov and V. A. Fateev, Parafermionic currents in the two-dimensional conformal quantum field theory and selfdual critical points in  $Z(n)$  invariant statistical systems, *ZhETF* **89**, 380 (1985) [*Sov. Phys. JETP* **62**, 215 (1985)].
- [63] H. Yi and C. L. Kane, Quantum Brownian motion in a periodic potential and the multichannel Kondo problem, *Phys. Rev. B* **57**, R5579(R) (1998).
- [64] H. Yi, Resonant tunneling and the multichannel Kondo problem: Quantum Brownian motion description, *Phys. Rev. B* **65**, 195101 (2002).
- [65] I. Affleck, M. Oshikawa, and H. Saleur, Quantum brownian motion on a triangular lattice and  $c = 2$  boundary conformal field theory, *Nucl. Phys. B* **594**, 535 (2001).
- [66] C. Nayak, S. H. Simon, A. Stern, M. Freedman, and S. Das Sarma, Non-Abelian anyons and topological quantum computation, *Rev. Mod. Phys.* **80**, 1083 (2008).
- [67] J. Alicea and P. Fendley, Topological phases with parafermions: Theory and blueprints, *Annu. Rev. Condens. Matter Phys.* **7**, 119 (2016).
- [68] T. K. T. Nguyen and M. N. Kiselev, Thermoelectric transport in a three-channel charge Kondo circuit, *Phys. Rev. Lett.* **125**, 026801 (2020).
- [69] W. Pouse, L. Peeters, C. L. Hsueh, U. Gennser, A. Cavanna, M. A. Kastner, A. K. Mitchell, and D. Goldhaber-Gordon, Quantum simulation of an exotic quantum critical point in a two-site charge Kondo circuit, *Nat. Phys.* **19**, 492 (2023).
- [70] D. B. Karki, E. Boulat, and C. Mora, Double-charge quantum island in the quasiballistic regime, *Phys. Rev. B* **105**, 245418 (2022).
- [71] D. B. Karki, E. Boulat, W. Pouse, D. Goldhaber-Gordon, A. K. Mitchell, and C. Mora,  $Z_3$  Parafermion in the double charge Kondo model, *Phys. Rev. Lett.* **130**, 146201 (2023).
- [72] L. Onsager, Reciprocal relations in irreversible processes. I., *Phys. Rev.* **37**, 405 (1931); Reciprocal relations in irreversible processes. II., **38**, 2265 (1931).
- [73] V. Zlatic and R. Monnier, *Modern Theory of Thermoelectricity* (Oxford University Press, New York, 2014).
- [74] G. Benenti, G. Casati, K. Saito, and R. Whitney, Fundamental aspects of steady-state conversion of heat to work at the nanoscale, *Phys. Rep.* **694**, 1 (2017).
- [75] D. B. Karki, Coulomb blockade oscillations of heat conductance in the charge Kondo regime, *Phys. Rev. B* **102**, 245430 (2020).
- [76] There is a missing factor  $2\pi$  in Eq. (13) of Ref. [35], which consequently requires us to put an additional prefactor  $2\pi$  in all formulas of thermoelectric coefficient  $G_T$  and thermopower  $S$  thereafter.
- [77] I. L. Aleiner and L. I. Glazman, Mesoscopic charge quantization, *Phys. Rev. B* **57**, 9608 (1998).
- [78] T. Giamarchi, *Quantum Physics in One Dimension* (Oxford University Press, Oxford, 2003).
- [79] Historically, the idea of double-large-dot charge Kondo configuration has been first theoretically proposed in Ref. [80] for the thermodynamic investigation of the fractional  $e/2$  charge Coulomb blockade capacitance peaks.
- [80] K. Le Hur, Fractional plateaus in the Coulomb blockade of coupled quantum dots, *Phys. Rev. B* **67**, 125311 (2003).
- [81] B. A. Jones and C. M. Varma, Study of two magnetic impurities in a fermi gas, *Phys. Rev. Lett.* **58**, 843 (1987); B. A. Jones, C. M. Varma, and J. W. Wilkins, Low-temperature properties of the two-impurity Kondo hamiltonian, *ibid.* **61**, 125 (1988).
- [82] J. Gan, Mapping the critical point of the two-impurity Kondo model to a two-channel problem, *Phys. Rev. Lett.* **74**, 2583 (1995); Solution of the two-impurity Kondo model: Critical point, Fermi-liquid phase, and crossover, *Phys. Rev. B* **51**, 8287 (1995).
- [83] A. K. Mitchell, E. Sela, and D. E. Logan, Two-channel Kondo physics in two-impurity Kondo models, *Phys. Rev. Lett.* **108**, 086405 (2012).
- [84] J. M. Luttinger, Theory of thermal transport coefficients, *Phys. Rev.* **135**, A1505 (1964).
- [85] B. S. Shastry, Electrothermal transport coefficients at finite frequencies, *Rep. Prog. Phys.* **72**, 016501 (2009).
- [86] F. G. Eich, M. Di Ventra, and G. Vignale, Density-functional theory of thermoelectric phenomena, *Phys. Rev. Lett.* **112**, 196401 (2014).
- [87] F. G. Eich, A. Principi, M. Di Ventra, and G. Vignale, Luttinger-field approach to thermoelectric transport in nanoscale conductors, *Phys. Rev. B* **90**, 115116 (2014).